

Dual lattice simulation of the U(1) gauge-Higgs model at finite density - an exploratory proof-of-concept study

Ydalia Delgado Mercado, Christof Gattringer, Alexander Schmidt

Institut für Physik, FB Theoretische Physik, Universität Graz, 8010 Graz, Austria

The U(1) gauge-Higgs model with two flavors of opposite charge and a chemical potential is mapped exactly to a dual representation where matter fields correspond to loops of flux and the gauge fields are represented by surfaces. The complex action problem of the conventional formulation at finite chemical potential μ is overcome in the dual representation and the partition sum has only real and non-zero contributions. We simulate the model in the dual representation using a generalized worm algorithm, explore the phase diagram and study condensation phenomena at finite μ .

PACS numbers: 11.15.Ha

Introductory remarks: In recent years lattice QCD has turned into a powerful quantitative tool in hadron physics. However, one aspect where lattice methods still face serious technical obstacles is QCD at finite density. The reason is that at finite chemical potential μ the action S is complex and the Boltzmann factor e^{-S} cannot be used as weight factor in a Monte Carlo simulation.

For some lattice models considerable progress was made by mapping the system to new (dual) degrees of freedom, where the partition sum has only real and positive terms (see [1–8] for examples related to this work). The dual variables are typically fluxes on the lattice that are subject to constraints. The worm algorithm [9] is a powerful tool for updating such constrained systems.

In this Letter we present a first proof-of-concept study for a system with gauge and matter fields at arbitrary couplings and finite density. We consider the U(1) gauge-Higgs model with two flavors and chemical potential. The corresponding dual representation is given in terms of closed loops of flux for the matter fields and surfaces for the gauge fields. For the Monte Carlo we compare two techniques and show that the dual approach successfully overcomes the complex action problem. We explore the phase diagram and as illustrative examples discuss Silver-Blaze type of transitions [10] and show that they can be understood as condensation of the dual variables.

U(1) gauge-Higgs model on the lattice: We here consider the model with two flavors of opposite charge described by complex scalar fields $\phi_x, \chi_x \in \mathbb{C}$ living on the sites x of the lattice. The gauge fields $U_{x,\sigma} \in \text{U}(1)$ live on the links. Throughout this paper we use 4-d euclidean lattices of size $V_4 = N_s^3 \times N_t$ with periodic boundary conditions for all directions. The lattice spacing is set to 1, i.e., all dimensional quantities are in units of the lattice spacing. Scale setting can be implemented as in any other lattice field theory and issues concerning the continuum behavior are, e.g., discussed in [11]. We write the action as the sum, $S = S_U + S_\phi + S_\chi$, where S_U is the gauge action and S_ϕ and S_χ are the actions for the two scalars. For the gauge action we use Wilson's form

$$S_U = -\beta \sum_x \sum_{\sigma < \tau} \text{Re} U_{x,\sigma} U_{x+\hat{\sigma},\tau} U_{x+\hat{\sigma},\sigma}^* U_{x,\tau}^*. \quad (1)$$

The sum runs over all plaquettes, $\hat{\sigma}$ and $\hat{\tau}$ denote the unit vectors in σ - and τ -direction and the asterisk is used for complex conjugation. The action for the field ϕ is

$$S_\phi = \sum_x \left(M_\phi^2 |\phi_x|^2 + \lambda_\phi |\phi_x|^4 - \sum_{\nu=1}^4 [e^{-\mu_\phi \delta_{\nu,4}} \phi_x^* U_{x,\nu} \phi_{x+\hat{\nu}} + e^{\mu_\phi \delta_{\nu,4}} \phi_x^* U_{x-\hat{\nu},\nu}^* \phi_{x-\hat{\nu}}] \right). \quad (2)$$

By M_ϕ^2 we denote the combination $8 + m_\phi^2$, where m_ϕ is the bare mass parameter of the field ϕ and μ_ϕ is the chemical potential, which favors forward hopping in time-direction (= 4-direction). The coupling for the quartic term is denoted as λ_ϕ . The action for the field χ has the same form as (2) but with complex conjugate link variables $U_{x,\nu}$ such that χ has opposite charge. M_χ^2 , μ_χ and λ_χ are used for the parameters of χ .

The partition sum $Z = \int D[U] D[\phi, \chi] e^{-S_U - S_\phi - S_\chi}$ is obtained by integrating the Boltzmann factor over all field configurations. The measures are products over the measures for each individual degree of freedom.

Note that for $\mu_\phi \neq 0$ (2) is complex, i.e., in the conventional form the theory has a complex action problem.

Dual representation: A detailed derivation of the dual representation for the 1-flavor model is given in [7] and the generalization to two flavors is straightforward. The final result for the dual representation of the partition sum for the gauge-Higgs model with two flavors is

$$Z = \sum_{\{p,j,\bar{j},l,\bar{l}\}} \mathcal{C}_g[p,j,l] \mathcal{C}_s[j] \mathcal{C}_s[l] \mathcal{W}_U[p] \mathcal{W}_\phi[j,\bar{j}] \mathcal{W}_\chi[l,\bar{l}]. \quad (3)$$

The sum runs over all configurations of the dual variables: The occupation numbers $p_{x,\sigma\tau} \in \mathbb{Z}$ assigned to the plaquettes of the lattice and the flux variables $j_{x,\nu}, l_{x,\nu} \in \mathbb{Z}$ and $\bar{j}_{x,\nu}, \bar{l}_{x,\nu} \in \mathbb{N}_0$ living on the links. The flux variables j and l are subject to the constraints \mathcal{C}_s (here $\delta(n)$ denotes the Kronecker delta $\delta_{n,0}$ and $\partial_\nu f_x \equiv f_x - f_{x-\hat{\nu}}$)

$$\mathcal{C}_s[j] = \prod_x \delta \left(\sum_\nu \partial_\nu j_{x,\nu} \right), \quad (4)$$

which enforce the conservation of j -flux and of l -flux at each site of the lattice. Another constraint,

$$\mathcal{C}_g[p, j, l] = \prod_{x, \nu} \delta \left(\sum_{\nu < \alpha} \partial_\nu p_{x, \nu \alpha} - \sum_{\alpha < \nu} \partial_\nu p_{x, \alpha \nu} + j_{x, \nu} - l_{x, \nu} \right), \quad (5)$$

connects the plaquette occupation numbers p with the j - and l -variables. At every link it enforces the combined flux of the plaquette occupation numbers plus the difference of j - and l -flux residing on that link to vanish.

The constraints (4) and (5) restrict the admissible flux and plaquette occupation numbers giving rise to an interesting geometrical interpretation: The j - and l -fluxes form closed oriented loops made of links. The integers $j_{x, \nu}$ and $l_{x, \nu}$ determine how often a link is run through by loop segments, with negative numbers indicating net flux in the negative direction. The flux conservation (4) ensures that only closed loops appear. Similarly, the constraint (5) for the plaquette occupation numbers can be seen as a continuity condition for surfaces made of plaquettes. The surfaces are either closed surfaces without boundaries or open surfaces bounded by j - or l -flux.

The configurations of plaquette occupation numbers and fluxes in (3) come with weight factors

$$\mathcal{W}_U[p] = \prod_{x, \sigma < \tau} I_{p_{x, \sigma \tau}}(\beta), \quad (6)$$

$$\mathcal{W}_\phi[j, \bar{j}] = \prod_{x, \nu} \frac{1}{(|j_{x, \nu}| + \bar{j}_{x, \nu})! \bar{j}_{x, \nu}!} \prod_x e^{-\mu j_{x, 4}} P_\phi(f_x),$$

with $f_x = \sum_\nu [|j_{x, \nu}| + |j_{x-\hat{\nu}, \nu}| + 2\bar{j}_{x, \nu} + 2\bar{j}_{x-\hat{\nu}, \nu}]$ which is an even number. The $I_p(\beta)$ in the weights \mathcal{W}_U are the modified Bessel functions and the $P_\phi(2n)$ in \mathcal{W}_ϕ are the integrals $P_\phi(2n) = \int_0^\infty dr r^{2n+1} e^{-M_\phi^2 r^2 - \lambda_\phi r^4} = \sqrt{\pi/16\lambda} (-\partial/\partial M^2)^n e^{M^4/4\lambda} [1 - erf(M^2/2\sqrt{\lambda})]$, which we evaluate numerically and pre-store for the Monte Carlo. The weight factors \mathcal{W}_χ are the same as the \mathcal{W}_ϕ , only the parameters M_ϕ^2 , λ_ϕ , μ_ϕ are replaced by M_χ^2 , λ_χ , μ_χ . All weight factors are real and positive. The partition sum (3) thus is accessible to Monte Carlo techniques, using the plaquette occupation numbers and the flux variables as the new degrees of freedom.

Observables and Monte Carlo update: In this exploratory study we consider first and second derivatives of the free energy as observables (for 2-point functions and spectroscopy in dual simulations see, e.g., [8]). In the dual language the observables are mapped into weighted sums over dual variables and their fluctuations [7].

The dual Monte Carlo update turns out to be rather simple. A detailed description is given in [7] and here we only introduce the key idea. The algorithm is a generalization of the worm algorithm [9] to surfaces with boundaries and we refer to it as *surface worm algorithm* (SWA). The SWA starts with violating the constraints at a randomly chosen link L_{defect} and the two sites at its endpoints by changing the occupation number of either

the j or the l variable at L_{defect} by ± 1 . Subsequently the occupation number p of one of the six plaquettes attached to L_{defect} is changed such that the violation of the constraint at L_{defect} is healed. Furthermore, for two of the other links of the plaquette the constraints are kept intact by changing the j or l fluxes on those links. Thus only at one link of the plaquette the constraints are still violated and this link is the new defect link L_{defect} . Iterating these steps the SWA propagates the defect link L_{defect} through the lattice until it terminates by inserting a final unit of j or l flux. Each step of the SWA is accepted with a local Metropolis decision. We use an additional step for updating loops of winding $j-l$ flux, and the unconstrained variables \bar{j} and \bar{l} are updated with conventional Metropolis sweeps.

We remark that for checking the correctness of the SWA we compare its results to a local algorithm in the dual representation [7] and for $\mu_\phi = \mu_\chi = 0$ also to a simulation in the conventional formulation.

Phase diagram at zero density: We begin with the analysis of the phase diagram and the properties of the different phases for the case of vanishing chemical potentials $\mu_\phi = \mu_\chi = 0$. This also serves as a test of the dual approach which at zero density can be compared to a conventional simulation. The other parameters are set to $M_\phi^2 = M_\chi^2 = M^2$ and $\lambda_\phi = \lambda_\chi = 1$ (fixed).

In Fig. 1 we show (left to right) the plaquette expectation value $\langle U \rangle$, the expectation value $\langle |\phi|^2 \rangle = 1/V_4 \partial \ln Z / \partial M_\phi^2$ and the particle number susceptibility $\chi_{n_\phi} = 1/V_4 \partial^2 \ln Z / \partial \mu_\phi^2$ versus β and M^2 . We remark that at $\mu = 0$ the particle number vanishes, but not χ_{n_ϕ} .

We use results from the dual approach for the 3-d mesh in Fig. 1 and for some of the parameter values superimpose data from a simulation in the conventional formulation to check the correctness of the dual representation (see [7] for a detailed comparison in the 1-flavor case).

For large mass parameter M^2 the matter fields decouple and the system is expected to display the (very weak) first order transition of pure U(1) lattice gauge theory from the confining to the Coulomb phase near $\beta \sim 1$. Indeed, for the largest value $M^2 = 8$ we see the behavior of $\langle U \rangle$ versus β as expected for the pure gauge case, and the critical value of β is very close to 1 (we studied this in more detail using the plaquette susceptibility – figures not shown). For vanishing β the theory reduces to a charged scalar field, which in the presence of a ϕ^4 -term has a transition to a Higgs phase. This strong first order transition is very pronounced in all three observables for our smallest coupling $\beta = 0.4$. It can be located using the maxima of the susceptibilities $\chi_U = 1/6V_4 \partial^2 \ln Z / \partial \beta^2$ and $\chi_{|\phi|^2} = 1/V_4 \partial^2 \ln Z / (\partial M_\phi^2)^2$, and with the inflection point of χ_{n_ϕ} . The result of this analysis is Fig. 2.

The first order line entering our range of parameters at $\beta = 0.4$ and $M^2 \sim 4.6$ (separating Higgs- and confining phase) shifts towards larger values of M^2 for increasing β until at $\beta \sim 1.0$, $M^2 \sim 6.6$ the visible jump in all three observables of Fig. 1 vanishes. From that point on a tran-

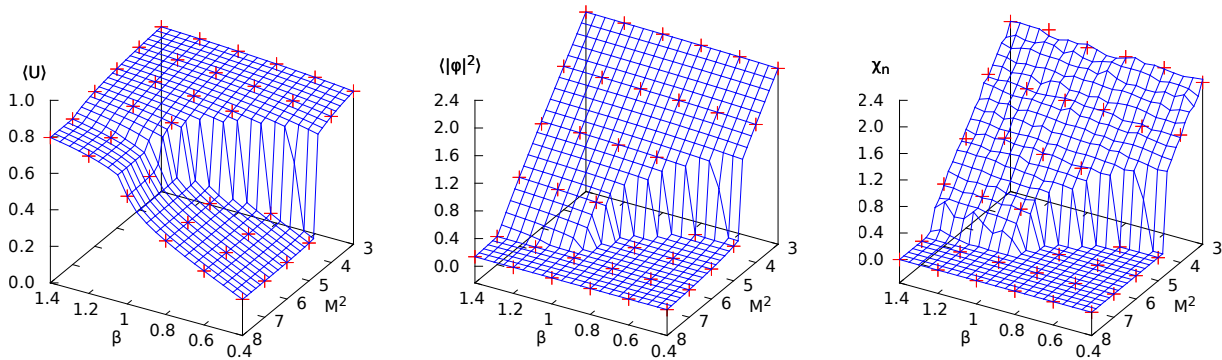


FIG. 1: The observables $\langle U \rangle$, $\langle |\phi|^2 \rangle$ and χ_{n_ϕ} (left to right) as function of the inverse gauge coupling β and mass parameter M^2 .

sition line that separates the confining- and the Coulomb phase continues towards the first order transition of pure gauge theory discussed above, which is visible in $\langle U \rangle$ and in $\langle |\phi|^2 \rangle$ (finer vertical scale is necessary for the latter observable). In addition we observe a transition line that separates the Higgs- and the Coulomb phase. It connects the branch point at $\beta \sim 1.0$, $M^2 \sim 6.6$, to $\beta = 1.4$, $M^2 \sim 6.9$ at the boundary of our parameter range. Thus we can distinguish three phases characterized by different values of $\langle U \rangle$, $\langle |\phi|^2 \rangle$ and χ_{n_ϕ} (see the labelling in Fig. 2).

We studied the different transition lines in Fig. 2 using finite size analysis of the second derivatives and histogram techniques, finding that the phase boundary separating Higgs- and confining phase is strong first order, the line separating confining- and Coulomb phase is of weak first order, and the boundary between Coulomb- and Higgs phase is a continuous transition. Our results for the $\mu = 0$ phase diagram are in qualitative agreement with the conventional results for related models [12].

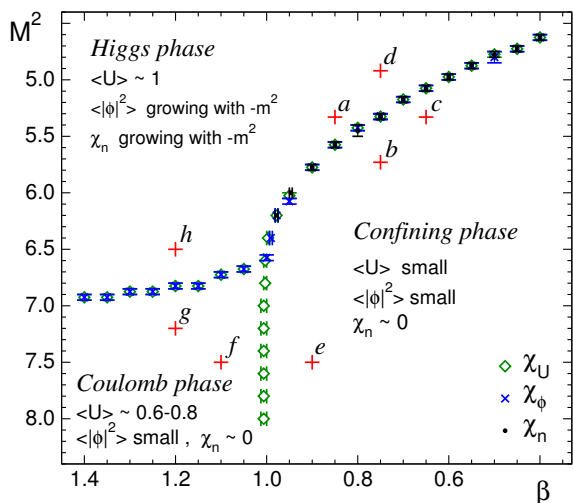


FIG. 2: Phase diagram in the β - M^2 plane at $\mu = 0$. We show the phase boundaries determined from the maxima of χ_U and χ_ϕ and the inflection points of χ_n . We also mark points where we performed runs at finite μ (plus-signs labelled a to h).

Analysis at finite density: Let us now come to the case of non-zero $\mu_\phi = \mu_\chi = \mu > 0$. Here the conventional formulation fails and we indeed need the dual approach for obtaining results. In Fig. 2 we mark 8 points (labelled a to h) in parameter space where we conducted simulations in the range $\mu \in [0, 5]$.

For 5 of them, points b , c , e , f and g we found very similar behavior with a strong first order transition as a function of μ which is visible in $\langle U \rangle$, n and $\langle |\phi|^2 \rangle$. As an example in the top row of Fig. 3 we show $\langle U \rangle$, $\langle |\phi|^2 \rangle$ and n as a function of μ for point b ($\beta = 0.75$, $M = 5.73$). All three observables jump at $\mu = \mu_c \sim 2.66$ from values characteristic for the $\mu = 0$ confining phase to values that correspond to the Higgs phase. We conclude that the finite μ transitions at the points b , c , e , f and g lead into the Higgs phase. This is consistent with the fact, that finite μ at tree level changes the mass $m^2 \rightarrow m^2 - \mu^2$, and thus also $M^2 \rightarrow M^2 - \mu^2$. This implies that for finite μ the transition into the Higgs phase takes place for larger values of M^2 , exactly as we observe. In other words, the phase boundary of the Higgs phase folds towards larger M^2 for increasing μ .

The points b , c , e , f and g have in common that they show a Silver-Blaze type of behavior [10] for their finite μ transition: In the corresponding range of parameters the $\mu = 0$ theory has a mass gap, and all observables are independent of μ until μ reaches the value of the mass of the lowest excitation. This behavior is clearly visible in the top row of Fig. 3. Furthermore, the transition can be seen to be accompanied by a condensation of dual variables. This is obvious from the top plot on the very right of Fig. 3, where we show the average plaquette number p , the average of $f_x = \sum_\nu [j_{x,\nu} + |j_{x-\hat{\nu},\nu}| + 2\bar{j}_{x,\nu} + 2\bar{j}_{x-\hat{\nu},\nu}]$ and the average flux l_4 in 4-direction (normalized with factors as given in the legend). All dual variables jump from very small values to finite numbers at $\mu_c \sim 2.66$.

The situation is different for the points a , d and h in the Higgs phase. There we have a Goldstone mode, i.e., no mass gap, and we expect a non-trivial μ -dependence for all values of μ . This behavior is evident in the bottom row plots of Fig. 3 where we show as a prototype example the μ dependence of the observables when starting from the

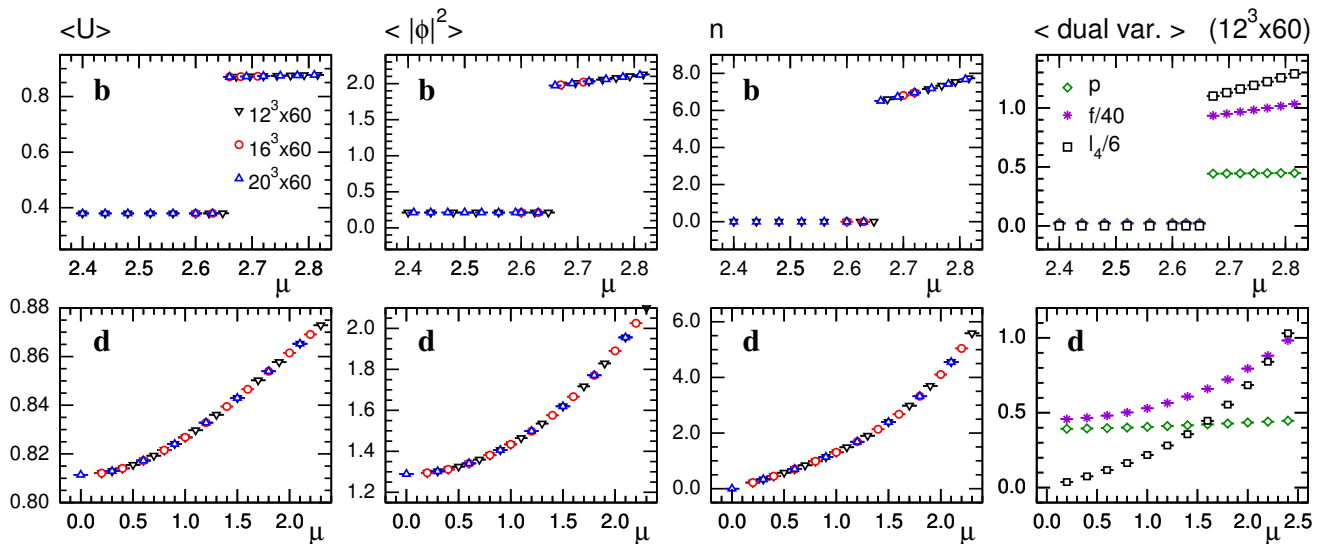


FIG. 3: From left to right we show the observables $\langle U \rangle$, $\langle |\phi|^2 \rangle$, n and the average dual variables (normalized with factors as given in the legends) as a function of μ for points b ($\beta = 0.75$, $M^2 = 5.73$, top row) and d ($\beta = 0.75$, $M^2 = 4.92$, bottom row).

Higgs phase for point d ($\beta = 0.75$, $M^2 = 4.92$). Here we do not observe discontinuities, but a roughly quadratic behaviour in μ , which can again be understood from the fact that the observables are essentially linear in $-m^2$ (see Fig. 1) and the mass shift $m^2 \rightarrow m^2 - \mu^2$. Also the dual variables show a continuous behaviour and do not condense (bottom row, plot at the very right).

We currently explore the location of the phase boundaries for a wide range of parameters, with the goal of an ab-initio study of the various phases suggested for the $U(1)$ gauge-Higgs system at finite μ [13].

Concluding remarks: In this exploratory study we have shown that the use of dual variables to overcome the complex action problem can be extended also to theories with gauge and matter fields, giving rise to surfaces for the gauge fields and loops that bound them for matter. The use of a generalized *surface worm algorithm* allows

for an efficient update and the analysis of the full phase diagram. The same structure of loops and surfaces is expected also for theories where the bosonic matter is replaced by fermions (although with additional minus signs for the loops). This is due to the fact that the fermion determinant can be expanded in loops dressed with gauge transporters and integrating out the gauge fields is then done in the same way as here. We expect that techniques tested in this paper will be developed further and be useful also for other systems with gauge and matter fields.

Acknowledgements: This work is supported by FWF DK 1203 "Hadrons in Vacuum, Nuclei and Stars", by DFG SFB TRR55 "Hadron Physics from Lattice QCD", by EU Research Executive Agency (REA), Grant PITN-GA-2009-238353, ITN "STRONGnet", and by EU FP7, Grant Nr. 283286, "Hadron Physics 3".

-
- [1] T. Sterling, J. Greensite, Nucl. Phys. B **220** (1983) 327. M. Panero, JHEP **0505** (2005) 066. V. Azcoiti, E. Follana, A. Vaquero, G. Di Carlo, JHEP **0908** (2009) 008. T. Korzec, U. Wolff, PoS LATTICE **2010** (2010) 029.
- [2] M.G. Endres, Phys. Rev. D **75** (2007) 065012; PoS LAT06 (2006) 133.
- [3] D. Banerjee, S. Chandrasekharan, Phys. Rev. D **81** (2010) 125007. C. Gattringer, A. Schmidt, Phys. Rev. D **86** (2012) 094506. P.N. Meisinger, M.C. Ogilvie, arXiv:1306.1495 [hep-lat].
- [4] S. Chandrasekharan, PoS LATTICE **2008** (2008) 003.
- [5] M. Fromm, J. Langelage, S. Lottini, O. Philipsen, JHEP **1201** (2012) 042. M. Fromm, J. Langelage, S. Lottini, M. Neuman, O. Philipsen, Phys. Rev. Lett. **110** (2013) 122001.
- [6] M. Hogervorst, U. Wolff, Nucl. Phys. B **855** (2012) 885. P. Weisz, U. Wolff, Nucl. Phys. B **846** (2011) 316.
- U. Wolff, Phys. Rev. D **79** (2009) 105002. T. Korzec, I. Vierhaus, U. Wolff, Comp. Phys. Comm. **182** (2011) 1477.
- [7] Y. D. Mercado, C. Gattringer, A. Schmidt, Comp. Phys. Comm. **184**, 1535 (2013).
- [8] C. Gattringer, T. Kloiber, Phys. Lett. B **720**, 210 (2013).
- [9] N. Prokof'ev, B. Svistunov, Phys. Rev. Lett. **87** (2001) 160601.
- [10] T.D. Cohen, Phys. Rev. Lett. **91** (2003) 222001.
- [11] M. Lüscher, P. Weisz, Nucl. Phys. B **290** (1987) 25; Nucl. Phys. B **295** (1988) 65; Nucl. Phys. B **318** (1989) 705.
- [12] K. Jansen, J. Jersak, C.B. Lang, T. Neuhaus, G. Vones, Nucl. Phys. B **265** (1986) 129; Phys. Lett. B **155** (1985) 268. K. Sawamura, T. Hiramatsu, K. Ozaki, I. Ichinose, arXiv:0711.0818 [cond-mat.str-el].
- [13] V. J. Peter, M. Sabir, Int. J. Mod. Phys. A **6** (1991) 4063; Mod. Phys. Lett. A **4** (1989) 783.